Optimal Design of Silicon-based Chips for Piezo-induced Ultrasound Resonances in Embedded Microchannels

Garofalo, F.; Laurell, T.; Bruus, Henrik

Published in:
Physics Procedia

Link to article, DOI:
10.1016/j.phpro.2015.08.039

Publication date:
2015

Document Version
Publisher's PDF, also known as Version of record

Available online at www.sciencedirect.com

ScienceDirect

Physics Procedia 70 (2015) 50 – 54

Physics Procedia

2015 International Congress on Ultrasonics, 2015 ICU Metz

Optimal design of silicon-based chips for piezo-induced ultrasound resonances in embedded microchannels

Garofalo F[a,*], Laurell T[a], Bruus H[b]

[a] *Department of Biomedical Engineering, Lund University, Ole Römers Väg 3 S-22363, Lund, Sweden*
[b] *Department of Physics, Technical University of Denmark, DK-2800 Kongens Lyngby, Denmark*

Abstract

We present a variational formulation of the governing equations and introduce global indicators to describe the behavior of acoustofluidic devices driven at resonance frequencies by means of a piezoelectric transducer. The individuation of the correct Lagrangian densities for the different parts constituting the device (the piezo transducer, the silicon walls, the fluid-filled microchannel, and the glass lid) allows for the introduction of the weak formulation used in the finite element discretization of the equations describing the system in its oscillatory regime. Additionally, the knowledge of the Lagrangian density leads to the derivation of the correct structure of the Hamiltonian density, i.e. the energy density, which is important for the quantification of the energy content of the whole system and its individual parts. Specifically, the energy content of the embedded microchannel is quantified by means of the acoustofluidic yield η defined as the ratio between the energy in the channel and the total energy. From the standpoint of acoustophoretic application, the introduction of the acoustophoretic mean orientation allows us to identify the frequencies for which an acoustophoretic effect, i.e. the lateral motion of particle dragged by the axial main flow, is particularly strong. Finally, the connection between the mechanical and electrical degrees of freedom of the system is addressed. This is important for proper determination of the dissipated power, and it may lead to the detection of resonance states by means of purely electrical measurements. Numerical simulations and preliminary experimental results show some features of the model introduced.

Peer-review under responsibility of the Scientific Committee of ICU 2015
Keywords:

1. Introduction

Acoustophoretic devices represent an efficient and easy-to-set-up method for the manipulation of biological samples. Indeed, this method has been shown to be able to manipulate cell lines as well as micrometric-sized beads (1; 2), by simply using an embedded microfluidic channel, or a capillary, in connection with the presence of a piezoelectric actuator that in the simplest cases can be glued to the structure containing the micro-channel (3). Despite the advantages in using this kind of technique with respect to other manipulation methods, e.g. (di-)electrophoresis and magnetophoresis, the identification of optimal working frequencies is yet entrusted with the presence of the operator, who has to search manually for resonance frequencies that afterwards can be tracked with the aid of electric mea-

* Corresponding author. Tel.: +0-000-000-0000
E-mail address: fabio.garofalo@bme.lth.se

Peer-review under responsibility of the Scientific Committee of ICU 2015
doi:10.1016/j.phpro.2015.08.039

surements. Furthermore, the design of acoustofluidic systems deserves additional investigations, since optimization of the geometric configuration of the device as well as the material properties can point out better ways to improve the effectiveness of the separation process and lead to a broadening of the range of applicability.

To this end, the present manuscript addresses objective global indicators that aid both the designer and the experimentalist to locate optimal working frequencies (4). The introduction of these global indicators is based upon a preliminary description of the equations governing the system in terms of Lagrangian densities. Specifically, the mechanical Lagrangian density features the parts of the system obeying to Helmoltz–Navier equation which describes elastic waves in the frequency domain. On the other hand, the acoustic Lagrangian density represents the propagation of acoustic pressure wave in the inviscid fluid, meaning that the corresponding governing equation is the Helmoltz wave equation for the pressure. Finally, the electro-mechanical Lagrangian density describes elastic waves in the piezoelectric element driven by the coupling to the dielectric behavior of the material in the presence of an imposed potential difference.

Addressing the exact form of the Lagrangian densities is important in two regards. First, the weak formulation of the governing equations for the finite element implementation stems directly from the individuation of the Lagrangian densities. This is important in the development of numerical methods that can be systematically checked by means of physical considerations. Second, the Hamiltonian density can be retrieved by splitting of the Lagrangian density in the kinetic and potential energy densities and summing them. The Hamiltonian density is important for the quantification of the system energy in all of the subsequent quantities, and it can be used to characterize the system both from the mechanical and electrical point of views.

Table 1. List of symbols.

ρ	Density	c	Speed of sound
$\boldsymbol{\varepsilon}$	Dielectric tensor	$\boldsymbol{P}$	Piezoelectric coupling matrix
$\boldsymbol{\Sigma}$	Stiffness tensor		
$\mathscr{L}$	Lagrangian density	$\mathscr{H}$	Hamiltonian density
$\boldsymbol{u}$	Displacement	p	Pressure
$\boldsymbol{\phi}$	Electric potential		
$\hat{L}$	Lagrangian	$\hat{H}$	Hamiltonian
$\hat{W}$	Work	$\hat{P}$	Power
L	Effective Lagrangian	H	Effective Hamiltonian
η	Acoustofluidic yield	α	Acoustophoretic mean orientation

2. Theory

The free Lagrangian densities, i.e. with no boundary contributions, for a system constituted by an elastic solid, an inviscid fluid, and a piezoelectric element driven at a given frequency in an oscillatory regime are

$$\mathscr{L}_{\mathrm{m}}(\boldsymbol{u}, \boldsymbol{\nabla u}) = \rho\omega^2 \boldsymbol{u}^* \cdot \boldsymbol{u} - \boldsymbol{\nabla u}^* : \boldsymbol{\Sigma} : \boldsymbol{\nabla u}, \tag{1}$$

$$\mathscr{L}_{\mathrm{a}}(p, \boldsymbol{\nabla} p) = \frac{\boldsymbol{\nabla} p^* \cdot \boldsymbol{\nabla} p}{\rho\omega^2} - \frac{p^* p}{\rho c^2}, \tag{2}$$

$$\mathscr{L}_{\mathrm{em}}(\boldsymbol{u}, \boldsymbol{\nabla u}, \phi, \boldsymbol{\nabla}\phi) = \rho\,\omega^2 \boldsymbol{u}^* \cdot \boldsymbol{u} - \boldsymbol{\nabla u}^* : \boldsymbol{\Sigma} : \boldsymbol{\nabla u} + \boldsymbol{\nabla}\phi^* \cdot \boldsymbol{\varepsilon} \cdot \boldsymbol{\nabla}\phi - 2\,\boldsymbol{\nabla}\phi^* \cdot \boldsymbol{P} : \boldsymbol{\nabla u}\,. \tag{3}$$

The meaning of the symbols appearing in these equations is given in table 1. We note that for the system we are considering, the field variables, i.e. the displacement, the pressure and the electric potential, should be labeled to address which subsystem of the device, they refer to. For the sake of clarity we omit this index to better illustrate the general idea of the variational framework. Thus, the corresponding Euler–Lagrange equations for the system of equations (1)–(3) that govern the behavior of the system in the oscillatory regime with angular frequency ω, can be retrieved by varying the Lagrangian densities with respect to the field variables $\boldsymbol{u}$, p, and ϕ. When we want to implement the governing equations in a finite element software, such as Comsol Multiphysics, we need just to provide the Lagrangian densities (1)–(3) and the boundary contributions to these. The latter are given by

$$\mathscr{L}_{\mathrm{m}}^{\mathrm{bnd}}(\boldsymbol{u}, \boldsymbol{\sigma}_{\mathrm{m}}^{\mathrm{bnd}}) = \boldsymbol{u}^* \cdot \boldsymbol{\sigma}_{\mathrm{m}}^{\mathrm{bnd}} \cdot \hat{\boldsymbol{n}}, \tag{4}$$

$$\mathscr{L}_{\mathrm{a}}^{\mathrm{bnd}}(p, \boldsymbol{u}_{\mathrm{f}}^{\mathrm{bnd}}) = p^* \, \boldsymbol{u}_{\mathrm{f}}^{\mathrm{bnd}} \cdot \hat{\boldsymbol{n}}, \tag{5}$$

$$\mathscr{L}_{\mathrm{em}}^{\mathrm{bnd}}(\boldsymbol{u}, \boldsymbol{\sigma}_{\mathrm{em}}^{\mathrm{bnd}}, \phi, \boldsymbol{d}_{\mathrm{em}}^{\mathrm{bnd}}) = \boldsymbol{u}^* \cdot \boldsymbol{\sigma}_{\mathrm{em}}^{\mathrm{bnd}} \cdot \hat{\boldsymbol{n}} - \phi^* \, \boldsymbol{d}_{\mathrm{em}}^{\mathrm{bnd}} \cdot \hat{\boldsymbol{n}}, \tag{6}$$

in the case of boundaries for that Dirichlet boundary conditions are assigned.

Remarkably, in the structure of the Lagrangian densities (1)–(3) the kinetic and the potential energy densities can be recognized and the derivation of the Hamiltonian densities is quite straightforward, being

$$\mathscr{H}_{\mathrm{m}} = \rho \, \omega^2 \boldsymbol{u}^* \cdot \boldsymbol{u} + \boldsymbol{\nabla u} : \boldsymbol{\Sigma} : \boldsymbol{\nabla u} \tag{7}$$

$$\mathscr{H}_{\mathrm{a}} = \frac{\boldsymbol{\nabla} p^* \cdot \boldsymbol{\nabla} p}{\rho \, \omega^2} + \frac{p^* p}{\rho \, c^2} \tag{8}$$

$$\mathscr{H}_{\mathrm{em}} = \rho \, \omega^2 \boldsymbol{u}^* \cdot \boldsymbol{u} + \boldsymbol{\nabla u}^* : \boldsymbol{\Sigma} : \boldsymbol{\nabla u} - \boldsymbol{\nabla} \phi^* \cdot \boldsymbol{\varepsilon} \cdot \boldsymbol{\nabla} \phi + 2 \, \boldsymbol{\nabla} \phi^* \cdot \boldsymbol{P} : \boldsymbol{\nabla u} \, . \tag{9}$$

With the aid of these densities, it is possible to compute the total energy of the system by integrating over the different parts of the devices, i.e. $\hat{H} = \int \mathscr{H} d\boldsymbol{x}$ and retrieving the effective value of the energy by means of the relation $H = \frac{1}{2}\Re[\hat{H}]$. Additionally, electrical related quantities can be computed, such as the Q-value, which is given by $Q = \Re[\hat{H}]/\Im[\hat{L}]$ and the (complex valued) impedance $\hat{Z} = i\phi_{\mathrm{app}}^2/\omega\hat{L}$, where ϕ_{app} is the potential applied to the piezo transducer. These expressions can be derived by considering the virtual work theorem and recognizing that the external power is given by $\hat{P} = -i\omega\hat{L}$ as well as $\hat{P} = \phi_{\mathrm{app}}\hat{I}$, where $\hat{I}$ is the complex valued current.

Electro-mechanical features alone do not provide information about the usability of a frequency in terms of acoustophoretic capabilities of the device. Therefore, we also introduce the *acoustofluidic yield*

$$\eta(\omega) = \frac{H_a(\omega)}{H(\omega)}, \tag{10}$$

being the ratio between the acoustic energy in the channel and total energy of the device, and the *acoustophoretic mean orientation*

$$\alpha(\omega) = \arctan \frac{\left\| \partial_y p(\boldsymbol{x}, \omega) \right\|_{L^1(\Omega_{\mathrm{channel}})}}{\| \partial_z p(\boldsymbol{x}, \omega) \|_{L^1(\Omega_{\mathrm{channel}})}}, \tag{11}$$

where $\|g\|_{L^1(\Omega)} = \int_\Omega |g^* g|^{1/2} \, d\Omega$ is the L^1-norm of the complex scalar field $g(\boldsymbol{x})$ for $\boldsymbol{x} \in \Omega$. This quantity provides a measure the inclination of the pressure wave vector with respect to the horizontal plane.

3. Results

Figure 1(a) shows the schematic of the acoustofluidic chip used in the numerical simulations. The chip is constituted by a piezoelectric element attached to a silicon structure in which an acoustofluidic channel has been etched. Finally, the top lid consists of Pyrex glass. A potential difference of 1 V is applied between the electrodes on the top and bottom edges of the piezo transducer. Note that since the Lagrangian depends on the square of the field variables, the energies scale with the square of the applied potential (the initial problem is linear). Figure 1(b) depicts the behavior of the acoustophoretic mean orientation (top dashed line), the logarithm of the energy (bottom blue line) and the acoustofluidic yield (bottom red line). Let us describe the method used to locate the optimal frequencies. The gray shaded area(s) are the *acoustophoretic bands*, that are the frequency intervals for which the acoustophoretic mean orientation is above a specified threshold θ, in this case $\theta = 0.9 \times \pi/2$. A mean orientation above this threshold is a necessary condition to observe an acoustophoretic effect, being the alignment of the particles along the vertical pressure node. Within these intervals, the energy states with a high amount of energy are candidates to produce an effective separation, these are the frequencies at which resonances occur namely the local maxima of the energy and can be termed as *the acoustophoretic energy peaks*. However, the occurrence of both of these conditions is not sufficient to ensure a strong acoustophoretic force. Indeed, since the system is compounded by different parts, it is not possible to say *a priori* where the energy is located. This third and last information is given by the *acoustofluidic yield* (or better the product of the acoustofluidic yield and the total energy) which allows to select between the acoustophoretic energy

peaks that have the maximum energy inside the channel. Therefore, predictions based on the total energy suggest an optimal frequency around 2.070 MHz, while if one considers the acoustofluidic yield the maximum is about 2.0 MHz. It must be noticed that informations about the acoustic energy content in the microchannel can be obtained by just measure displacement of particles by means of optical methods, e.g. μ-PIV, while informations about the energy content of the whole system can be obtained by means of electrical measurements.

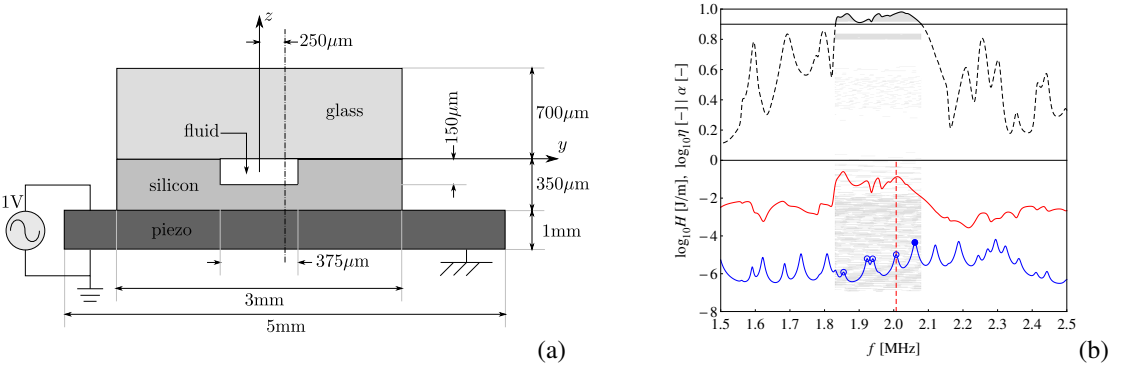

Fig. 1. (a): Schematic of the cross-section of the acoustophoretic device used in the numerical simulations. (b): Behavior of the normalized acoustophoretic mean orientation $2/\pi\,\alpha$ (top axes), the energy $\log_{10} H$ (bottom axes, blue line) and the acoustofluidic yield $log_{10}\eta$ (bottom axes, red line) as function of the excitation frequency f. Symbols are the acoustophoretic energy peaks (filled symbol is the optimum according to H) and the vertical dashed red line is the optimal working frequency.

In order to show preliminary results for the accordance of numerical predictions compared to experiments, figure 2(a) reports the orientation, the energy and the yield relatives to simulations of an acoustophoretic device similar to that depicted in figure 1(a), except for the channel width and the piezo displacement, that in this new case are 300 μm and 1 mm, respectively. The graph depicts also the *focusability* of the chip. This quantity has been computed by statistical analysis of the particle position recorded by means of fluorescence images. Panel (b) and (c) in figure 2 show two examples of these images in the case of unfocused (b) and focused (c) particle streams. Panel (a) shows that the optimal acoustophoretic frequency derived from numerical simulations agrees very well with the maximum of the focusability, and in general the predictions of the acoustophoretic bands in the range $f = 2.3 \div 2.5$ MHZ agree with the result of the focusability experiments.

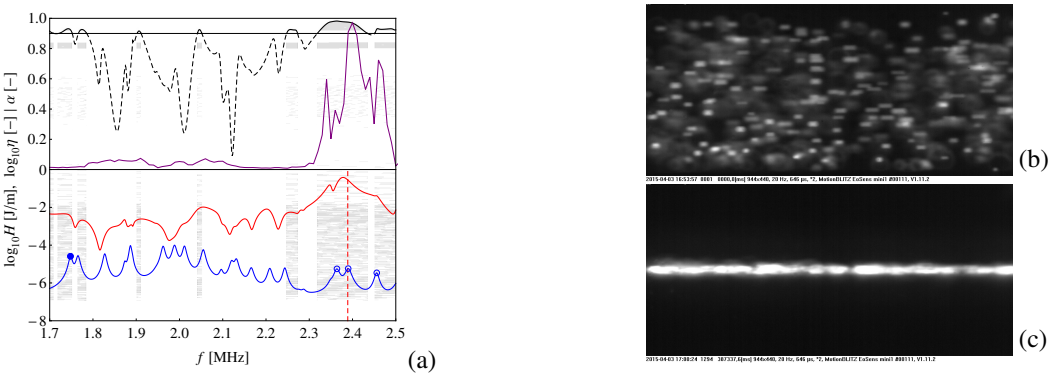

Fig. 2. (a): Behavior of the normalized acoustophoretic mean orientation $2/\pi\,\alpha$ (top axes), the energy $\log_{10} H$ (bottom axes, blue line) and the acoustofluidic yield $log_{10}\eta$ (bottom axes, red line) as function of the excitation frequency f. Symbols are the acoustophoretic energy peaks (filled symbol is the optimum according to H) and the vertical dashed red line is the optimal working frequency. Purple line is the focusability of the device. (b) & (c): Fluorescence images used in the derivation of focusability parameter.

4. Concluding Remarks

In this paper a variational model for the characterization of optimal working frequency for acoustophoretic devices has been introduced. The model allows to compute for the mechanical and electrical features of the device and the mathematical connection between these. Acoustophoretic orientation and acoustofluidic yield provide the additional informations to characterize the device in terms of acoustophoretic capabilities. A rationale for the detection of optimal frequencies has been addressed by introducing acoustophoretic bands and acoustophoretic energy peaks. Finally, preliminary experimental results have shown the agreement of the numerical simulations for a frequency sweep and a specific configuration of the acoustophoretic device.

References

[1] A. Lenshof, C. Magnusson and T. Laurell, *Acoustofluidics 8: Applications of acoustophoresis in continuous flow microsystems.* Lab Chip (2012) 12: 1210.

[2] M. Evander and J. Nilsson, *Acoustofluidics 20: Applications in acoustic trapping.* Lab Chip (2012) 12: 4667.

[3] M. Edge and M. Hill, *Acoustofluidics 17: Theory and applications of surface acoustic wave devices for particle manipulation.* Lab Chip (2012) 12: 2998.

[4] F. Garofalo, T. Laurell and H. Bruus, *Energy characterization of frequency spectra for electrically-actuated silicon/glass acoustophoretic devices.* Phys Rev E (to be submitted).

[5] F. Garofalo, O. Jakobsson, C. Antfolk, H. Bruus and T. Laurell, *Bridging simulations and experiments by quantitative analysis of effective focusing frequencies in proto-typical acoustophoretic devices.* μ-TAS 2015 (submitted).